Carrier dynamics in hybrid nanostructure with electronic couplingfrom an InGaAs quantum well to InAs quantum dots

Ying Wang*, Xinzhi Sheng

School of Science, Beijing Jiaotong University, Beijing 100044, P. R. China

Qing Yuan, Qinglin Guo, Shufang Wang, Guangsheng Fu

College of Physics Science & Technology, Hebei University, Baoding 071002, P.R. China

Baolai Liang*, Diana L Huffaker

California NanoSystem Institute, University of California - Los Angeles, CA 90095, U.S.A.

Yuriy I. Mazur, Yurii Maidaniuk, Morgan E. Ware, Gregory J. Salamo

Institute for Nanoscience and Engineering, University of Arkansas, AR 72701

*Corresponding to: hbuwangying@126.com and liangbaolai@gmail.com

Abstract: Carrier dynamics including carrier relaxation and tunneling within a coupled InAs quantum dot (QD) – $In_{0.15}Ga_{0.85}As$ quantum well (QW) hybrid nanostructure are investigated using photoluminescence (PL) spectroscopy. This coupled hybrid nanostructure shows a single PL peak from the QD emission at low excitation intensity and a band filling behavior is observed as the excitation intensity increases, suggesting that there exists a channel to capture carriers from the QW to the QDs. Time resolved PL (TRPL) measurements extract a carrier tunneling time of 103.7ps, which is only one third of the theoretical prediction. A double-channel resonant carrier tunneling mechanism from the QW to the wetting layer and to the fifth excited state of the QDs and then carrier relaxation into lower discrete QD energy states is proposed to explain this fast

carrier tunneling. The double-channel resonant carrier tunneling mechanism is qualitatively supported through the analysis of the excitation-dependent PL spectra as well as the PL excitation spectra. These results enrich our understanding of carrier dynamics in coupled QD and QW hybrid structures.

Keywords: carrier dynamics; resonant carrier tunneling; photoluminescence; quantum dots; quantum well.

1. INTRODUCTION

Since 1993, self-assembled quantum dots (QDs) grown by the Stranski-Krastanow (S-K) strain relaxation have gained great attention due to their possible optoelectronic device applications, such as semiconductor lasers, amplifiers, modulators, photovoltaic, and infrared photo-detectors [1-6]. As examples, QD hybrid structures with QDs coupled to a quantum well (QW) have been exploited in various material systems and optoelectronic devices where additional excess carriers can be provided through carrier transfer from the QW [7-14]. There are at least two ways to fabricate such QD hybrid systems. The first, a so-called dot in well (DWELL) structure, immerses QDs directly into a QW. This has been well studied and used to modify the performances for QD lasers, photodetectors, and intermediate-band solar cells [15-18]. A second approach is to architect the "injection-structure" by separating the QD layer from the QW with a thin barrier. This approach is particularly interesting because it allows for more independent control of the QDs, as well as the ability to inject carriers from the QW to the QDs [19-22]. The nanostructures obtained via this second approach have been explored most recently to improve

the device performance for lasers and photovoltaics [22, 23]. In view of the significance of the applications and the complexities of the structures, carrier dynamics play a very important role in the improvement of device performances while carrier injection and processes involved in vertical and lateral transfer have been well investigated for several hybrid systems. In this paper, we report comparison studies on two hybrid structures with InAs QDs coupled and uncoupled to an InGaAs QW. The emission characteristics for these two samples are investigated by excitation intensity and temperature dependent PL together with time-resolved PL (TRPL). A fast carrier tunneling is experimentally observed and a double-channel resonant carrier tunneling mechanism from the QW to the wetting layer and to the discrete energy states of the QDs is proposed to explain the observed fast carrier tunneling.

2. SAMPLE STRUCTURES AND MBE GROWTH

The hybrid structures were grown by a solid source molecular beam epitaxy (MBE). As shown in Fig. 1(a), for the coupled sample A, a 500nm GaAs buffer layer was grown on a semi-insulating GaAs (001) substrate at 580°C, then a 15 nm $In_{0.15}Ga_{0.85}As$ QW layer grown at a substrate temperature of 520°C, followed by a 3 nm GaAs spacer at 520°C and 1.8 monolayers (ML) of InAs at 520°C which form QDs through S-K relaxation, and finally a 150 nm GaAs capping layer was grown at 580°C. An uncoupled sample B was grown using the same growth conditions except that the QD and QW layers are inverted in the layer order with a 160 nm spacer between them, as shown in Fig. 1(b). This inversion was chosen in order that the QW PL is not absorbed by the lower energy QDs. With the assumptions that the QD layer is pseudomorphic,

i.e., introduces no new defects, and that the 160nm spacer is sufficiently large such that strain from the QDs do not influence the growth of the QW, we believe that this inversion will have no other effects on the results.

As reference, a sample with QDs formed from the deposition of 1.8 ML of InAs at 520°C and no capping is grown for morphology study by Atomic Force Microscope (AFM). As shown in Figure 1(c), the uncapped QDs were measured to have an areal density of $\sim 4.8\times10^{9}cm^{-2}$, an average height of 11.5 nm, and an average diameter of 46.8 nm. Defects or large incoherent islands are not found on the surface of the sample, indicating high quality, pseudomorphic QDs. It is well known that the dimensions and shape of the InAs QDs will change significantly after the QDs are capped. As shown in Figure 1(d), the cross-sectional Transmission Electron Microscopy (TEM) images show much smaller InAs QDs with a diameter of ~20 nm and a height of ~2.5 nm for both sample A and sample B in comparison with the QDs observed by AFM. The QD dimensions measured by TEM rather than by AFM were subsequently used to obtain reasonable band structure calculations using the semiconductor simulation package, Nextnano. The coupled structure between QDs and QW via a 3nm GaAs spacer is also confirmed for sample A by the TEM images.

3. RESULTS AND DISSCUSSION

For PL measurements, samples were excited by a continuous-wave 532 nm laser, i.e., with energy is well above the GaAs band gap. Therefore, the photon-excited carriers are mainly generated in the GaAs matrix, then relax into the QW and the QDs. The PL spectra for both

samples were first measured at low temperature (T=10K) with the low excitation intensity of 10mW/cm^2 to avoid saturation effect. As shown in Fig. 1(e), sample A has a single peak from QD emission at 1.103 eV with a Full-Width-at-Half-Maximum (FWHM) of 27meV. In comparison, sample B has shown a QD peak at 1.087 eV with a FWHM of 27 meV and a narrow QW peak at 1.390 eV with a FWHM of 9meV. Here we find that the PL from the QDs in both samples have very similar emission energy and linewidth. However, we will show that the QW peak from Sample A is absent due to rapid carrier transfer to the QDs.

Subsequently, examining the PL as a function of laser excitation intensity shows how the available states fill and emit. This is shown in Figs. 2 (a) and 2(b) for samples A and B, respectively. We see here, that the overall structure of the excitation intensity dependencies from these two samples are generally quite similar in that they both show a classical state filling progression of the QD peaks. However, we find that the states fill remarkably faster with increasing power in sample A where the QDs and QW are coupled than they do in sample B where they are uncoupled. Additionally, the initially absent QW peak from sample A appears at ~1.39eV and increases in intensity rapidly. Finally, at the highest excitation intensities, we see a high energy shoulder become prominent at ~1.43eV in both samples. This is most likely the emission from the QD wetting layer or the excited states of the QW. Due to the quick increase in intensity of the QW peak in sample A, we conclude that there is an efficient channel for carrier relaxation from the GaAs matrix to the QW and then to the QDs [24]. Therefore, it is only after the QDs are sufficiently filled that the QW emission peak turns on. Here, the QW plays the role of a reservoir to efficiently collect photon-generated carriers from the GaAs matrix and pass them

to the QDs, although the carrier generation and carrier relaxation in the QW as well as in the QDs also exist. Following this, the carriers begin to quickly populate the QW energy states after the lower energy levels of the QDs have been filled, according to the calculated band diagram shown in Fig.2(c).

The integrated PL intensity of the QW and of the QDs for sample B, as well as their ratio (QW/QDs) are extracted and plotted in Fig. 2 (d) as a function of the laser excitation intensity. In general, the relationship between the integrated PL intensity for quantum structures and the laser excitation intensity can be described by the power law [25-27], $I_{PL} = \eta \times P^{\alpha}$, where P is the excitation laser intensity, and α and η are fitting coefficients. By fitting the experimental data, the coefficient α is found to be approximately equal to unity in both case, indicating that the main contributing mechanism is exciton recombination for both QD and QW [26]. However, the QW and QDs show different values for η. This is closely related to the PL efficiency [25]. For the uncoupled sample B, we obtain $\eta=1.75\times10^3$ for the QDs and $\eta= 2.2\times10^3$ for the QW, which indicates that this sample has a better carrier collection efficiency for the QW than the QDs in the low excitation regime. We also observed that the integrated PL intensity ratio (QW/QDs) increases slowly in the low excitation regime. However, after the QD energy states become saturated at ~30 W cm^{-2}, the ratio increases sharply. This is mostly due to the much larger density of states of the QW and the fact that it requires a much larger excitation intensity to get an emission saturation than the QDs. Therefore, an InGaAs QW is suitable to host more carriers to work as the carrier reservoir for providing carriers to the QDs.

In Fig. 2 (e) the QD integrated PL intensities are extracted in the low excitation regime for both samples. Again, the integrated PL intensity of the QDs can be described by the power law, $I_{PL} = \eta \times P^{\alpha}$. By fitting the experimental data, the coefficient α is again found to be approximately equal to unity for the QDs in both samples, indicating an exciton recombination mechanism. However, we obtain $\eta=2.06\times10^3$ for the coupled sample and $\eta=1.75\times10^3$ for the uncoupled sample, indicating a better carrier collection/emission efficiency for the QDs of coupled sample A in the low excitation regime. As mentioned above, the carrier transfer from the QW to the QDs provides additional carriers for the QDs. In this case, the coupled sample A should have stronger QD emission signal than the uncoupled sample B under the same excitation intensity. We measured that the QD PL intensity of sample A is ~2.3 times larger than that of sample B under an excitation intensity of 0.01 W/cm^2.The measured QD PL intensity ratio of sample A over sample B is always larger than 1 over 3 orders of magnitude change of excitation intensity from 0.01 W/cm^2 to 10 W/cm^2. However, each sample has different thickness of GaAs capping layer on top of the QDs, we cannot directly use the measured PL intensity to label QD emission efficiency. Therefore, the integrated PL intensity ratio between QDs in the coupled sample A and the QDs in the uncoupled sample B is extracted and we found it decreases with respect to the excitation intensity. This is an indication that there is efficient transfer of carriers between the QW and the QDs, as this decrease in ratio indicates that the QDs in the coupled sample approach saturation faster due to the additional source of carriers from the QW.

The assumption of carrier transfer from the QW to the QDs through the 3nm GaAs spacer is built into the calculated band structure in Fig. 2(c). This is further supported by the spectral

profile analysis in Fig. 2(f) showing sample A under 300W/cm^2 of excitation. Here we see an obvious multiband structure with well-resolvable QD excited states labeled E_1, E_2, E_3, E_4, and E_5. The fitted Gaussians are uniformly separated by~56meVwith linewidths of 38~53meV. Figs. 2(c) and 2(f) indicate that the ground electron state of the QW, E^0_{QW}, is approximately resonant with the fifth excited state the QDs, E_5. By careful comparison of the PL spectra under strong excitation from both samples in Fig. 2(g) and Fig. 2(h), we found that the QW of the coupled sample A has a much broader linewidth than that of the uncoupled QW FWHM of 9 meV as seen in Fig 2(h), sample B. Therefore, we suggest that in Fig. 2(g) the strong, broadened PL peak at ~1.39eV is the result of a combination of several possible factors in addition to the E^0_{QW} emission. These may include emission from light hole states, mixed QD and QW states, as well as the E_5 states of the QDs. This creates an obvious pathway for resonant tunneling transfer of carriers between the E^0_{QW} state of the QW to E_5 state the QDs with subsequent relaxation in the QDs to E_0.

To further characterize the carrier transfer from QW to QDs, PL excitation (PLE) spectra were measured at 10 K using a super-continuum laser with the detection set at the maximum of the QD PL band for each sample. As shown in Fig. 3(a), the PLE spectra from both samples reveal clear excitation resonances at 1.51 eV due to the GaAs matrix. However, only Sample A shows a resonance at ~1.39 eV, which matches the InGaAs QW emission energy and therefore indicates resonance carrier transfer from the QW to the QDs. In addition, in order to observe the detailed features of this resonant PLE peak, we plotted in Fig. 3(b) the QW PL spectra measured at 300W/cm^2 together with zoomed PLE spectra at around the QW wavelength range that is indicated by the dash line rectangle in Fig. 3(a). Here we find that this resonant enhancement in

the PLE spectrum has a FWHM narrower than the QD excited state E_5, but broader than the QW PL peak (FWHM=9 meV). This supports the idea that the PL peak at ~1.39eV is a combination of the emission from several sources. This broadening has previously been used as a signature for the hybridization of tunnel-coupled QW/QD states [28-29].

The PLE spectra in Fig. 3(b) demonstrate two very interesting features. First, the resonant enhancement at ~1.39 eV reveals a strong carrier transfer from the QW to QDs for the coupled sample A [22]. This confirms the role of the QW as a carrier reservoir from which more carriers are captured into the QDs. Second, a splitting of several meV is observed in the PLE resonance in Fig. 3(b). Such a splitting is expected if one assumes resonant tunneling between the QW and QDs resulting in hybridization of the involved electronic states [29]. As the strength of the resonantly enhanced tunneling is determined by the thickness of the GaAs spacer layer that separates the QD and QW structure, we speculate that our hybrid structure with a 3nm GaAs thin spacer falls into the strong coupling regime. This strong coupling leads to the formation of hybridized electronic states which are spatially delocalized across the QW/QD interface [28].

The PL spectral curves in Fig. 2(g) and 2(h) together with the PLE spectra in Fig. 3(b) reveal more features at the QW energy of ~1.39eV and wetting layer energy of ~1.42eV. Calculations of the QW energy structure in Nextnano along with the PLE measurements of the uncoupled sample B also established that the first excited state of the QW, E^1_{QW}, and the QD WL electron state are nearly resonant, which is expected to lead to further significantly enhanced coupling between the QW and the QDs for the thin 3nm spacer. Therefore, a possible double-channel resonant carrier tunneling mechanism from the E^0_{QW} to the wetting layer and from the E^1_{QW} to the 5^{th} excited

state of the QDs, exists in this hybrid structure. Due to the special double-channel resonant carrier tunneling, the carriers can rapidly stream from the QW into the QD states, resulting in the observed vanishing intensity of the QW PL signal at low excitation power. Thus, the resonant coupling transforms the QW into a reservoir that supplies and controls the flux of carriers to the QDs from the GaAs barrier. This double-channel resonant carrier tunneling mechanism can result in a fast carrier tunneling time that will be measured by TRPL and be discussed later.

Figure 4 summarizes the temperature dependence of the PL spectra. In Fig. 4 (a) the integrated PL intensity as a function of temperature reveals two regions for the coupled sample A. With an excitation intensity of 100 W/cm^2, from 10 K to ~200 K the integrated intensity decreases only slowly with increasing temperature, demonstrating the strong three-dimensional confinement effect and larger exciton binding energy for the InAs QDs [24]. Above ~200 K, accelerated thermal escape from QDs is seen in the rapid drop in integrated intensity with increasing temperature. At the same time, the uncoupled sample B shows three different regions. From 10 K to ~40 K the integrated PL intensity is stable. When the temperature reaches above ~50 K, there is an increase for the QD integrated PL intensity, while at the same time the QW integrated intensity starts to decrease rapidly. After the temperature increases to above ~80 K, the integrated PL intensity of the QDs shows similar characteristicsto the coupled sample A in Fig. 4 (a). Clearly, the temperature where the QW integrated PL intensity begins to rapidly decrease is experimentally observed to depend on the pump intensity.

The temperature-dependent features of the integrated PL intensity for the uncoupled sample B can be understood through the localization of carriers [24, 27]. The low binding energy of the

excitons in the QW can be seen by the decay of intensity starting at ~50K. However, the concurrent increase in intensity of the QD PL indicates a transfer of carriers from the QW to the QDs. Therefore, we propose that the thermally excited carriers from the QW diffuse towards the QDs and are recaptured, thus increasing the QD emission intensity. This becomes another source of carriers for the lower energy QDs, which is effectively turned off for the lower temperatures studied in Fig. 2. Additionally, Fig. 4(c) shows the PL peak energy shift of the QD ground state and the QW as a function of temperature for both samples. We find that the coupled sample A shows a larger red-shift than the uncoupled sample B. This also due to the carrier transfer for sample A.

Finally, TRPL is measured for both samples at 10 K using a streak camera system with a temporal resolution of ~35ps. The samples are excited by a Ti:Sapphire mode-locked laser (780 nm, 78 MHz, 2.7 picosecond pulse) while the emission is detected with a C5680 Hamamatsu streak camera with an infrared-enhanced photocathode. The decay curves are measured at the QW and QD peak wavelengths for both samples with an excitation intensity of ~ 4×10^6 photons/pulse to avoid saturation effects. By fitting the decay curves, we extract the carrier lifetime.

We first discuss the lifetime for sample B. As indicated by Fig. 5(b), both the QDs and the QW PL peaks exhibit a mono-exponential decay behavior. By fitting the decay curves, the carrier lifetimes of the QW and QDs are measured to be τ_{QW}= 470 ps and τ_{QD}= 1400 ps, respectively, which agree well with reported values [30]. The lifetime for sample A demonstrates, though, a very different mechanism. As shown in Fig. 5(a), although the QDs still show a similar mono-

exponential decay behavior with a lifetime of τ_{QD}= 1450 ps, similar to sample B, the QW PL shows a multi-exponential decay behavior with an effective lifetime of τ_{QW}= 85 ps, which is nearly an order of magnitude faster than that from sample B. This means that, for carriers in the QW of the coupled sample A, carrier transfer is in strong competition with radiative recombination. As an additional evidence, the QD PL intensity reaches its maximum at t=245ps, while the QW obtains its maximum intensity at t=175ps. It is likely that the QW feeds additional carriers to the QDs, modifying the carrier relaxation process resulting in the QW and QDs reaching their maximal intensities at different times. In contrast, for the uncoupled sample B shown in Fig. 5(b), both the QW and QD emissionrise simultaneously to obtain the maximum intensity at t=175ps each only due to the photo-generated carriers from the laser pulse.

We can model the transfer of carriers between the QW and the QDs in sample A by examining a simple three-level system, i.e., a system with two separate decay paths [31-32]. Here, the measured PL decay time, τ_{PL}, for the QW is approximately given by:

$$\tau_{\mathrm{PL}} = \tau_{\mathrm{s}} \cdot \frac{\tau_t}{\tau_s + \tau_t} \qquad (1),$$

where τ_t is the carrier tunneling time from the QW to the QDs and τ_s is the radiative lifetime of carriers in the QW. From the experimental data shown in Fig. 5 and using equation (1), we estimate the carrier tunneling time, τ_t, to be 103.7 ps.

Additionally, we can also estimate the carrier tunneling time for this sample using a modified form of the semi-classical Wentzel–Kramers–Brillouin (WKB) approximation [33-36]. In this approximation τ is given by:

$$\tau = \frac{1}{vT} = \frac{m^*}{8\hbar} \cdot \frac{\rho_0^4}{\kappa_0^2 K_0^3} \cdot \omega \cdot \exp(2\kappa_0 b) \quad (2),$$

Here $\nu = \frac{\hbar\kappa_0}{2m^*\omega}$ is the quasi-classical collision frequency of the carriers, $T = \frac{16\kappa_0^2 K_0^2}{\rho_0^4} \cdot \exp(2\kappa_0 b)$ is the transmissivity of electrons passing through the potential barrier. Additionally we have: $\kappa_0 = \sqrt{2m^*(V_0 - E_0)}/\hbar$, $K_0 = \sqrt{2m^* E_0}/\hbar$, and $\rho_0 = \sqrt{2m^* V_0}/\hbar$, where b is the thickness of barriers, V_0 is the height of barriers, and E_0 is the intrinsic energy of the bound states. Using Eq. (2), the carrier tunneling time is calculated to be τ~350ps. The calculated carrier tunneling time is three times longer than the experimentally measured time, τ_t = 103.7 ps. As mentioned above, this fast carrier tunneling time suggests a resonant carrier transfer from the QW to the QDs. In particular, a possible double-channel resonant carrier tunneling mechanism from the E^0_{QW} to the wetting layer and from the E^1_{QW} state to the 5th excited state of the QDs could further reduce the lifetime of carriers in the QW. This assumption is built into the calculated band structure in Fig. 2(c) and is supported by the PLE measurement in Fig. 3(b) for sample A. It should also be mentioned the measured short carrier lifetime at ~1.39eV indicates that it is not a pure QW signal, but possible a combination of emission from several different states, including E^0_{QW}, the light hole state, the mixed state, and the E_5 state from the QDs.

The PL, PLE, and TRPL measurements demonstrate that for the coupled sample A, there is an efficient channel for carrier relaxation from the GaAs matrix to the QW and then to the QDs. Due to the additional carriers provided by the QW, the coupled sample A has a stronger QD emission efficiency than the uncoupled sample B. The most common mechanisms for carrier

transfer between two neighbor quantum structures is the short-range carrier tunneling due to quantum coupling and the long-range transfer of exciton energy due to the Forster coupling. From the AFM shown in Figure 1, the average center-to-center separation between the neighbor QDs was estimated to be more than 80 nm. For such a big separation, experimental and theoretical investigations have proved that both mechanisms for direct exciton transfer along lateral directions between the QDs are neglected. Therefore, we conclude that the nature of the carrier transfer in our hybrid structures is the short-range carrier tunneling due to quantum coupling from the InGaAs QW to InAs QDs along the vertical direction [37-38].

For this QD-QW hybrid nanostructure, the above results clearly indicate that there is quantum mechanical coupling leading to vertical carrier transfer from the InGaAs QW to the InAs QDs. This vertical coupling is strongly related to the GaAs spacer thickness and the energy separation (i.e., the indium content in the QW as well as the QW width) between the QW and the ground state energy state of the InAs QDs. For a similar coupled structure with a 3nm spacer, previous reports have determined it to be in the strong coupling or medium coupling regime [28-29]. Based on our PL and PLE results, we believe that our hybrid nanostructure is in the strong coupling regime, where the electron wave-function or the electron probability density is smeared out from both the QW and the QD confining potentials to penetrate into each other. As a result, a very fast carrier tunneling time from the QW into the QDs is experimentally observed [39-40]. Also, the broadening as well as splitting of the resonance peak have been experimentally observed as a signature for the hybridization of tunnel-coupled QW/QD states.

4. CONCLUSIONS

In summary, photoluminescence of coupled and uncoupled hybrid structures with a single layer of InAs QDs adjacent to an $In_{0.15}Ga_{0.85}As$ QW have been comparatively investigated. For the coupled structure, discrete emission peaks from the QD energy states, the QW, wetting layer, and the GaAs matrix are observed to consequently appear as the excitation intensity increases. At the same time, the PLE spectra and modeling band structure reveal a double-channel resonant carrier tunneling mechanism from the E^0_{QW} state to the wetting layer and from the E^1_{QW} state to the 5th excited state of the QDs. TRPL demonstrates that there is a strong competition between the carrier transfer and radiative recombination within the QW for the coupled sample. The coupled QW is found to have a very short carrier lifetime of 85ps due to the resonant carrier transfer from the QW to the wetting layer and the excited state of the QDs, after which the carriers relax into discrete QD energy states. These properties identify the coupled nature of the system as distinct from the properties of the uncoupled system due to fast carrier tunneling from the QW to the InAs QDs though the thin 3 nm GaAs spacer.

Acknowledgement: This research is supported by the Natural Science Foundation of People's Republic of China (Grant# 61575016 &Grant# 61774053) and the National Science Foundation of the U.S. (EPSCoR Grant # OIA-1457888). The authors acknowledge the support by Dr. Subhananda Chakrabarti and Vijay Ahire at Indian Institute of Technology-Bombay on the Nextnano modeling.

References:

1. Z. Yuan, B. E. Kardynal, R. M. Stevenson, A. J. Shields, C. J. Lobo, K. Cooper, N. S. Beattie, D. A. Ritchie, M. Pepper, Electrically driven single-photon source, *Science* 295:102-105 (2002).

2. X. Q. Li, Y. W. Wu, D Steel, D. Gammom, T. H. Stievater, D. S. Katzer, D. Park, C. Piermarocchi, L. J. Sham, An all-optical quantum gate in a semiconductor quantum dots, *Science* 301:809-811 (2003).

3. H. Y. Liu, T. Wang, Q. Jiang, R. Hogg, F. Tutu, F. Pozzi, A. Seeds, Long-wavelength InAs/GaAs quantum-dot laser diode monolithically grown on Ge substrate, *Nature Photonics* 5: 416-419 (2011).

4. Z. Mi, P. Bhattachaya, S. Fathpour, High-speed 1.3um tunnel injection quantum-dot lasers, *Appl. Phys. Lett*. 86: 153109 (2005).

5. J. Wu, X. Hu, J. Lee, E.-.S. Kim, Z. M. Wang, Epitaxially Self-Assembled Quantum Dot Pairs, *Adv. Opt. Mater.* 1:201-214 (2013).

6. B. L. Liang, P. S. Wong, D. L. Huffaker, T. Tran, C. K. Shih, V. G. Dorogan, Yu I. Mazur, M. E. Ware, G. J. Salamo, Site-controlled formation of InGaAs quantum nanostructures - tailoring the dimensionality and the quantum confinement, *Nano Research* 6: 235-242 (2013).

7. H. D. Lu, F. M. Guo, B. Zhang, W. G. Ning, Optical storage behavior in InAs quantum dots embedded in GaAs quantum well structure, *Micro & Nano Letters*, 11:623–626, (2016).

8. S. Wolde, Y. F. Lao, A. G. Unil Perera, Y. H. Zhang, T. M. Wang, J. O. Kim, T. Schuler-Sandy, Z. B. Tian, and S. Krishna, Noise, gain, and capture probability of p-type InAs-GaAs

quantum-dot and quantum dot-in-well infrared photodetectors, *J. Appl. Phys.* 121: 244501 (2017).

9. P. Bhattachaya, M. Zhang, J. Hinckley, Tunnel injection $In_{0.25}Ga_{0.75}N$/GaN quantum dot light-emitting diodes, *Appl. Phys. Lett*. 97: 251107 (2010).

10. H. S. Lee, K. H. Lee, J. C. Choi, H. L. Park, T. W. Kim, and D. C. Choo, Enhancement of the activation energy in coupled CdTe/ZnTe quantum dots and quantum-well structures with a ZnTe thin separation barrier, *Appl. Phys. Lett.* 81: 3750-3752 (2002).

11. X. B. Zhang, J. H. Ryou, R. D. Dupuis, G. Walter, N. Holonyak Jr., Temperature-dependent luminescence of InP quantum dots coupled with an InGaP quantum well and of InP quantum dots in a quantum well, *Appl. Phys. Lett.*87:201110 (2005).

12. W. Rudno-Rudziński, G. Sęk, K. Ryczko, M. Syperek, J. Misiewicz, E. S. Semenova, A. Lemaitre, and A. Ramdane, Room temperature free carrier tunneling in dilute nitride based quantum well -quantum dot tunnel injection system for 1.3μm, *Appl. Phys. Lett.* 94: 171906 (2009).

13. M. Pieczarka, M. Syperek, D. Bieganska, C. Gilfert, E. M. Pavelescu, J. P. Reithmaier, J. Misiewicz, and G. Sek, Lateral carrier diffusion in InGaAs/GaAs coupled quantum dot-quantum well system, *Appl. Phys. Lett.* 110, 221104 (2017).

14. M. Biswas, S. Singh, A. Balgarkashi, R. L. Makkar, A. Bhatnagar, N.B.V. Subrahmanyam, S. K. Gupta, P. Bhagwat, S. Chakrabarti, Ultra-thin GaAsN matrix-induced reduced full width at half maximum of GaAsN/InAs/GaAsN dot-in-a-well heterostructures with extended emission wavelength, *J. Lumin.* 194: 341-345 (2018).

15. J. Tatebayashi, A. Khoshakhlagh, S. H. Huang, G. Balakrishnan, L. R. Dawson, D. L. Huffaker, D. A. Bussian, H. Htoon, and V. Klimov, Lasing characteristics of GaSb/GaAs self-assembled quantum dots embedded in an InGaAs quantum well, *Appl. Phys. Lett.* 90:261115 (2007).

16. H. Y. Liu, M. J. Steer, T. J. Badcock, D. J. Mowbray, M. S. Skolnick, P.Navaretti, K. M. Groom, M. Hopkinson, and R. A. Hogg, Long-wavelength light emission and lasing from InAs/GaAs quantum dots covered by a GaAsSb strain-reducing layer, *Appl. Phys. Lett.* 86: 143108 (2005).

17. M. C. Debnath, T. D. Mishima, M. B. Santos, Y. Cheng, V. R. Whiteside, I. R. Sellers, K. Hossain, R. B. Laghumavarapu, B. L. Liang, and D. L. Huffaker, High-density InAs/$GaAs_{1-x}Sb_x$ quantum-dot structures grown by molecular beam epitaxy for use in intermediate band solar cells, *J. Appl. Phys.* 119: 114301 (2016).

18. A. Agarwal, S. Krishna and S. Chakrabarti, Investigation of thermal interdiffusion in InAs/$In_{0.15}Ga_{0.85}As$/GaAs Quantum Dot-in-a-Well heterostructures, *J. Lumin*. 143: 96-100, (2013).

19. K. M. Goodfellow, C. Chakraborty, K. Sowers, P.Waduge, M.Wanunu, T. Krauss, K. Driscoll, A. N. Vamivakas, Distance-dependent energy transfer between CdSe/CdS quantum dots and a two dimensional semiconductor, *Appl. Phys. Lett*. 108: 021101 (2016).

20. W. Rudno-Rudziński, M. Syperek, J. Andrzejewski, A. Maryński, J. Misiewicz, A. Somers, S. Höfling, J. P. Reithmaier, and G. Sęk, Carrier delocalization in InAs/InGaAlAs/InP quantum-dash-based tunnel injection system for 1.55 μm emission, *AIP Advances* 7: 015117 (2017).

21. O. D. D. Couto Jr., P. T. de Almeida, G. E. dos Santos, M. A. G. Balanta, H. F. Andriolo, J. A. Brum, M. J. S. P. Brasil, and F. Iikawa, B. L. Liang, and D. L. Huffaker, Carrier dynamics dictated by bimolecular recombination in type-II quantum dots coupled to quantum wells, *J. Appl. Phys.* 120: 084305 (2016).

22. R. B. Laghumavarapu, B.L. Liang, Z. Bittner, T. S. Navruz, S. Hubbard, D. L. Huffaker, GaSb/InGaAs quantum dot-well hybrid structures as active regions in solar cells, *Sol. Energy Mater Sol. Cells*, 114: 165-171 (2013).

23. L. V. Asryan, Effect of pumping delay on the modulation bandwidth in double tunneling-injection quantum dot lasers, *Opt. Lett*. 42:97 (2017).

24. P. S. Wong, B. L. Liang, V. G. Dorogan, A. R. Albrecht, J. Tatebayashi, X. He, N Nuntawong, Yu I. Mazur, G J Salamo, S R J Brueck, D L Huffaker, Improved photoluminescence efficiency of patterned quantum dots incorporating a dots-in-the-well structure, *Nanotechnology*. 19:435710 (2008).

25. S. R. Jin, Y. L. Zheng, A. Z. Li, Characterization of photoluminescence intensity and efficiency of free excitonsin semiconductor quantum well structures, *J. Appl. Phys.* 82:3870–3873 (1997).

26. S. Martini, A. A. Quivy, A. Tabata, J. R. Leite, Influence of the temperature and excitation power on theoptical properties of InGaAs/GaAs quantum wells grown on vicinal GaAs(001) surfaces, *J. Appl. Phys.* 90: 2280–2289 (2001).

27. Y. J. Ma, Y. G. Zhang, Y. Gu, S. P. Xi, X. Y. Chen, B. L. Liang, B. C. Juang, D. L. Huffaker, B. Du, X. M. Shao, J. X. Fang, Behaviors of beryllium compensation doping in InGaAsP grown by gas source molecular beam epitaxy, *AIP Adv.* 7: 075117 (2017).

28. M. Syperek, J. Andrzejewski, W. Rudno-Rudzinski, G. Sek, J. Misiewicz, E. M. Pavelescu, C. Gilfert, and J. P. Reithmaier, Influence of electronic coupling on the radiative lifetime in the (In,Ga)As/GaAs quantum dot–quantum well system, *Phys. Rev. B*85: 125311 (2012).

29. Yu. I. Mazur, V. G. Dorogan, E. Marega Jr., M. Benamara, Z. Ya. Zhuchenko, G. G. Tarasov, C. Lienau, and G. J. Salamo, Excited state coherent resonant electronic tunneling in quantum well-quantum dot hybrid structures, *Appl. Phys. Lett.* 98: 083118 (2011)

30. X. D. Mu,Y. J. Ding, B. S. Ooi, M. Hopkinson, Investigation of carrier dynamics on InAs quantum dots embedded in InGaAs⁄GaAsquantum wells based on time-resolved pump and probe differential photoluminescence, *Appl. Phys. Lett.*89:181924 (2006).

31. B. L. Liang, Zh. M. Wang, Yu. I. Mazur, G. J. Salamo, Photoluminescence of surface InAs quantum dot stacking on multilayer buried quantum dots, *Appl. Phys. Lett.* 89:243124 (2006).

32. Yu. I. Mazur, Zh. M. Wang， G. G. Tarasov, M. Xiao, G. J. Salamo, J. W. Tomm, V. Talalaev, Interdot carrier transfer in asymmetric bilayer InAs/GaAs quantum dot structures, *Appl. Phys. Lett*.86:063102 (2005).

33. A. Tackeuchi, T. Kuroda, K. Mase, Y. Nakata, N. Yokoyama, Dynamics of carrier tunneling between vertically aligned double quantum dots, *Phys. Rev. B.* 62:1568-1571 (2000).

34. Y. Zhang, H. Zheng, Tunneling escape time of electrons from a quantum well with Γ-X mixing effect, *Appl. Phys. Lett*.65:1036-1038 (1994).

35. Y. Zhang, H. Zheng, Study on electron tunneling escape time from quantum well, *J Infrared Millim Waves.* 13:69-72 (1994).

36. Y. Liu, B. L. Liang, Q. L. Guo, S. F. Wang, G. S. Fu, N. Fu, Yu. I. Mazur, M. E. Ware, G. J. Salamo, Electronic coupling in nanoscale InAs/GaAs quantum dot pairs separated by a thin Ga(Al)As spacer, *Nanoscale Res. Lett.* 10:271 (2015).

37. M. Syperek, P. Leszczyński, J. Misiewicz, E. M. Pavelescu, C. Gilfert, and J. P. Reithmaier, Time-resolved photoluminescence spectroscopy of an InGaAs/GaAs quantum well-quantum dots tunnel injection structure, *Appl. Phys. Lett.*96: 011901 (2010).

38. Yu. I. Mazur, V. G. Dorogan, E. Marega Jr., Z. Ya. Zhuchenko, M. E. Ware, M. Benamara, G. G. Tarasov, P.Vasa, C. Lienau, and G. J. Salamo, Tunneling-barrier controlled excitation transfer in hybrid quantum dot-quantum well nanostructures, *J. Appl. Phys.*108: 074316 (2010).

39. D. Guzun, Yu. I. Mazur, , V. G. Dorogan, M. E. Ware, E. Marega Jr., G. G. Tarasov, C. Lienau, and G. J. Salamo, Effect of resonant tunneling on exciton dynamics in coupled dot-well nanostructures, *J. Appl. Phys.* 113: 154304 (2013).

40. S. L. Chen, T. Kiba, X. J. Yang, J. Takayama, and A. Murayama, Power-dependent spin amplification in (In,Ga)As/GaAs quantum well via Pauli blocking by tunnel-coupled quantum dot ensembles, *Appl. Phys. Lett.*108: 152103 (2016).

Captions

Figure 1 (a) and (b) are the schematic diagrams of the hybrid structures for coupled sample A and uncoupled sample B, respectively; (c) 0.5 μm × 0.5 μm AFM image of the InAs QDs with an enlarged 3D view; (d) TEM images of InAs QDs in both samples A and B; (e) and (f) show the PL spectra of the two samples measured at T=10K with an excitation intensity of P=10mW/cm^2.

Figure 2 (a) and (b) show the low-temperature PL spectra of the two samples measured with excitation intensity from P=I_0=3mW/cm^2 to P=$10^6 I_0$; (c) Calculated band diagram for the hybrid structure showing the InAs QDs and $In_{0.15}Ga_{0.85}As$ QW; (d) shows the integrated PL intensities of the QW and the QDs for the uncoupled sample B together with the intensity ratio (QW/QD) as a function of the laser intensity; (e) shows the integrated PL intensity of the QDsin both samples together with their ratio (QD_A/QD_B) as a function of the laser intensity; (f) shows the Gaussian fitting analysis of the PL spectrum measured at T=10K with a strong excitation intensity of P=$10^5 I_0$=300W/cm^2; (g) and (h) show the QW PL spectra as a function of the excitation intensity for each sample, respectively.

Figure 3. (a) PL spectra measured at P=30mW/cm^2 and PLE spectra for both samples are plotted for low temperature (T=10K); (b) PL spectra measured at P=300W/cm^2 and PLE spectra zoomed in to the QW wavelength range indicated by the dash line rectangle in Fig. 3(a).

Figure 4. Integrated PL intensities of (a) the coupled sample A and (b) the uncoupled sample B as functions of temperature at different excitation intensities. (c) the energy shift of the PL peaks as functions of temperature.

Figure 5. TRPL results for (a) the coupled sample A and (b) the uncoupled sample B.

Figure 1

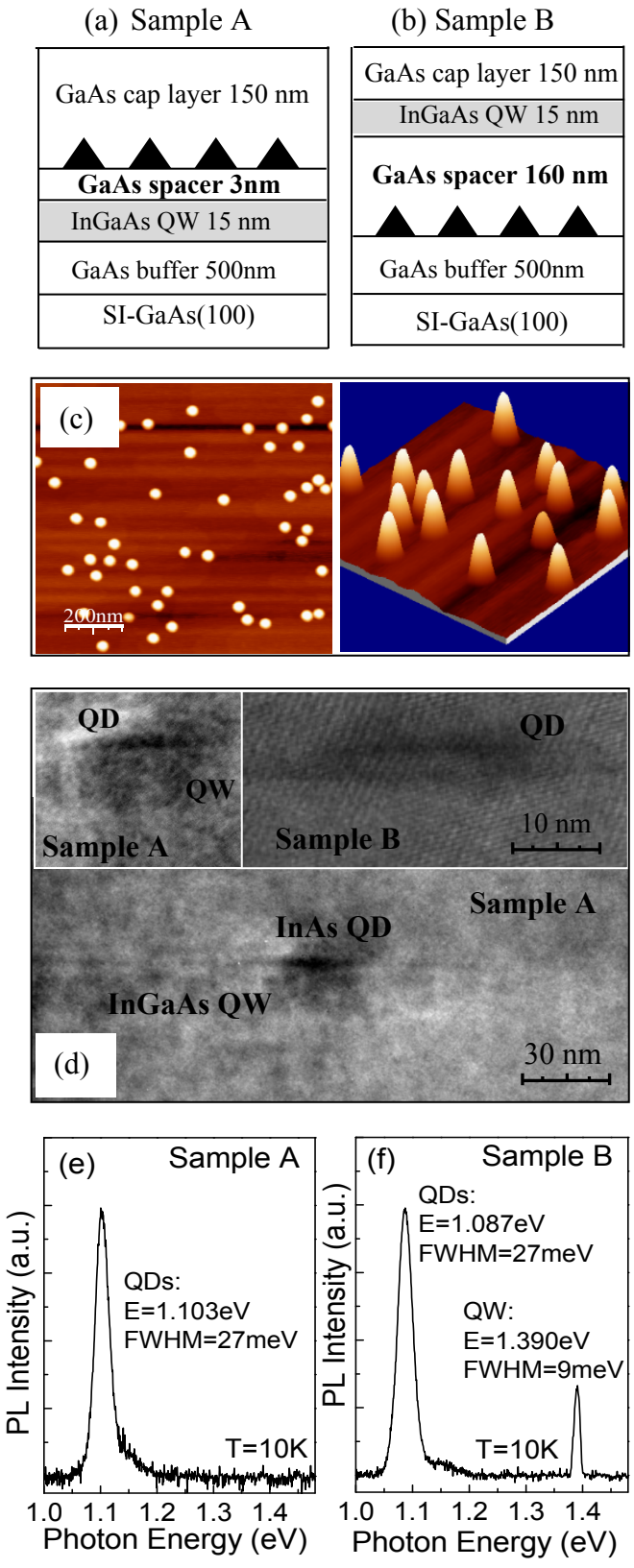
(a) Sample A
GaAs cap layer 150 nm
GaAs spacer 3nm
InGaAs QW 15 nm
GaAs buffer 500nm
SI-GaAs(100)
(b) Sample B
GaAs cap layer 150 nm
InGaAs QW 15 nm
GaAs spacer 160 nm
GaAs buffer 500nm
SI-GaAs(100)
(c)
200nm
QD
QW
Sample A
QD
Sample B
10 nm
Sample A
InAs QD
InGaAs QW
(d)
30 nm
(e)
Sample A
QDs:
E=1.103eV
FWHM=27meV
T=10K
PL Intensity (a.u.)
1.0 1.1 1.2 1.3 1.4
Photon Energy (eV)
(f)
Sample B
QDs:
E=1.087eV
FWHM=27meV
QW:
E=1.390eV
FWHM=9meV
T=10K
PL Intensity (a.u.)
1.0 1.1 1.2 1.3 1.4
Photon Energy (eV)

Figure 2

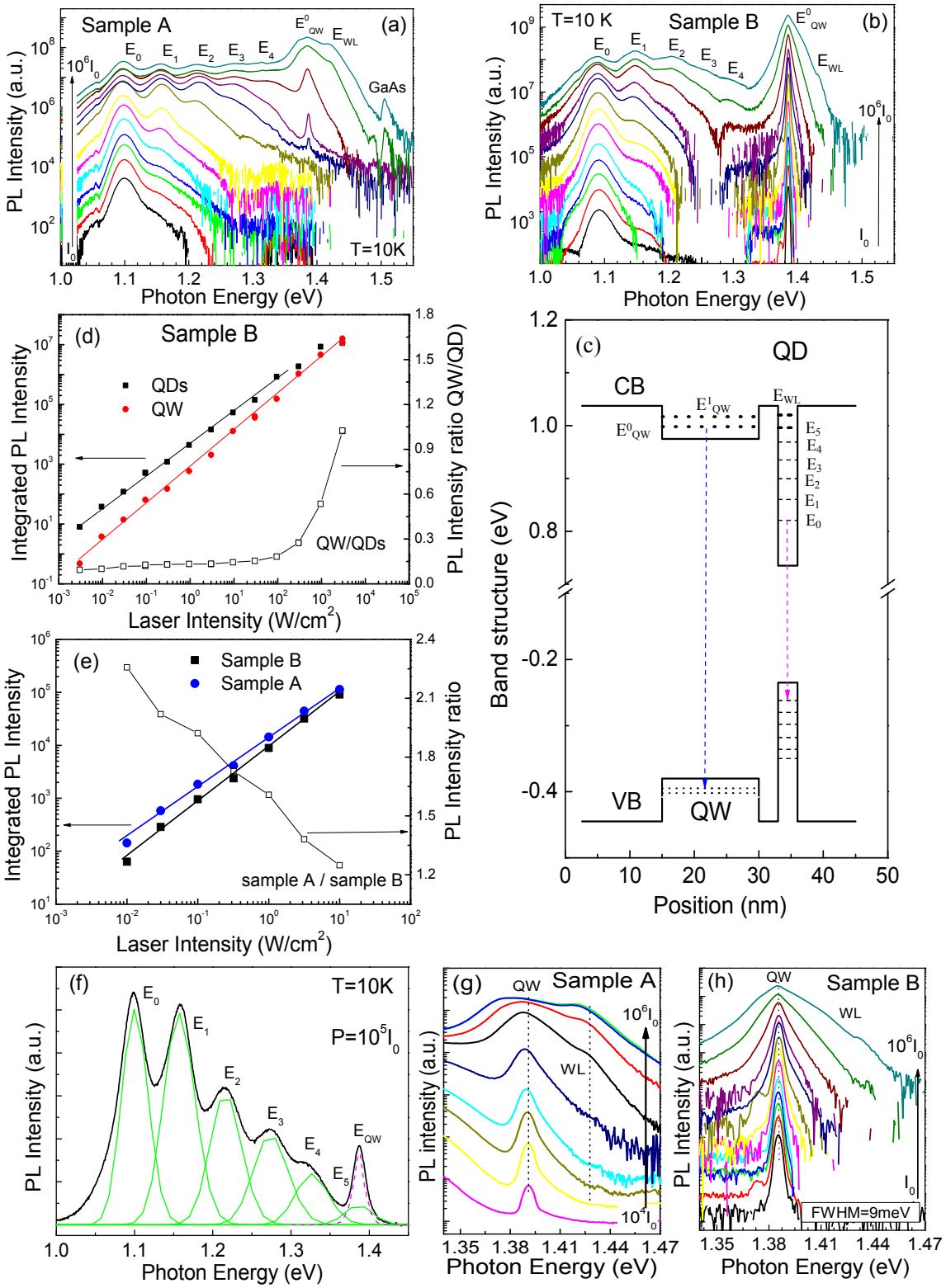
Sample A
(a)
T=10K
GaAs
PL Intensity (a.u.)
Photon Energy (eV)
T=10 K
Sample B
(b)
(d)
QDs
QW
QW/QDs
Integrated PL Intensity
PL Intensity ratio QW/QD
Laser Intensity (W/cm2)
(c)
QD
CB
VB
QW
Band structure (eV)
Position (nm)
(e)
Sample B
Sample A
sample A / sample B
PL Intensity ratio
(f)
T=10K
P=10^5 I0
(g)
QW
Sample A
WL
PL intensity (a.u.)
(h)
Sample B
FWHM=9meV

Figure 3

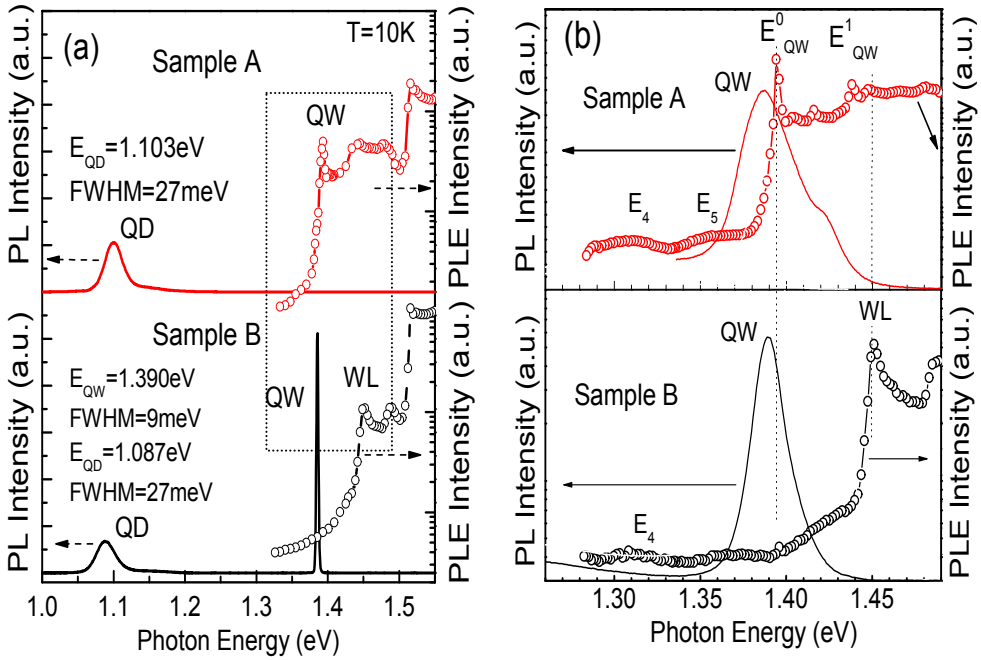
(a)
Sample A
T=10K
QW
E_{QD}=1.103eV
FWHM=27meV
QD
Sample B
E_{QW}=1.390eV
FWHM=9meV
E_{QD}=1.087eV
FWHM=27meV
QD
QW
WL
PL Intensity (a.u.)
PLE Intensity (a.u.)
1.0
1.1
1.2
1.3
1.4
1.5
Photon Energy (eV)
(b)
E^0_{QW}
E^1_{QW}
Sample A
QW
E_4
E_5
Sample B
QW
WL
E_4
1.30
1.35
1.40
1.45
Photon Energy (eV)

Figure 4

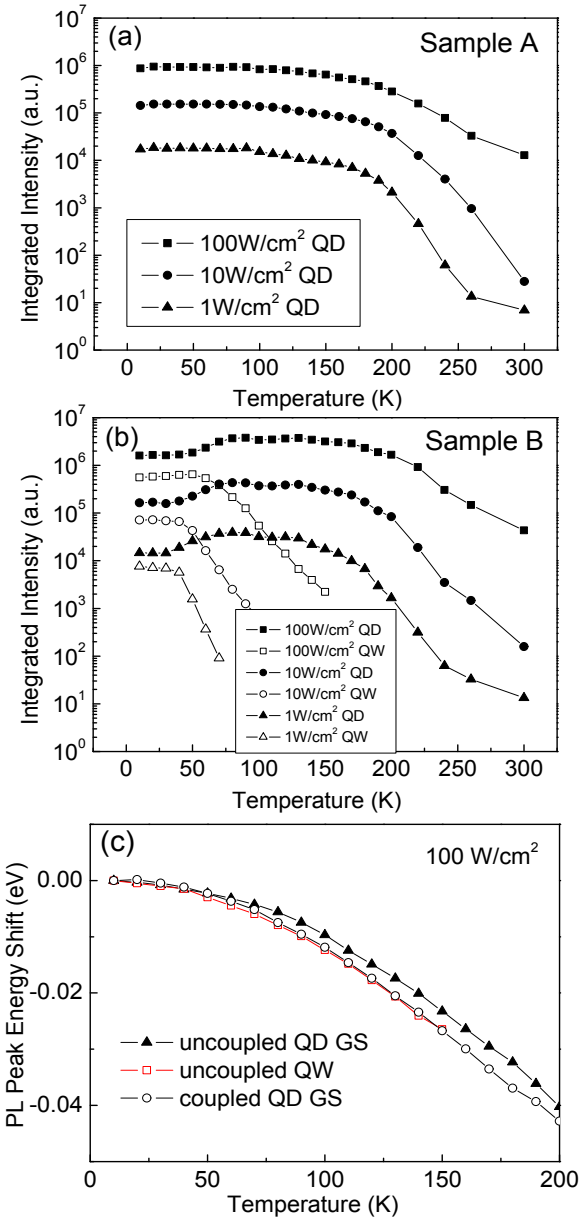
(a)
Sample A
Integrated Intensity (a.u.)
100W/cm² QD
10W/cm² QD
1W/cm² QD
Temperature (K)
(b)
Sample B
Integrated Intensity (a.u.)
100W/cm² QD
100W/cm² QW
10W/cm² QD
10W/cm² QW
1W/cm² QD
1W/cm² QW
Temperature (K)
(c)
100 W/cm²
PL Peak Energy Shift (eV)
uncoupled QD GS
uncoupled QW
coupled QD GS
Temperature (K)

Figure 5

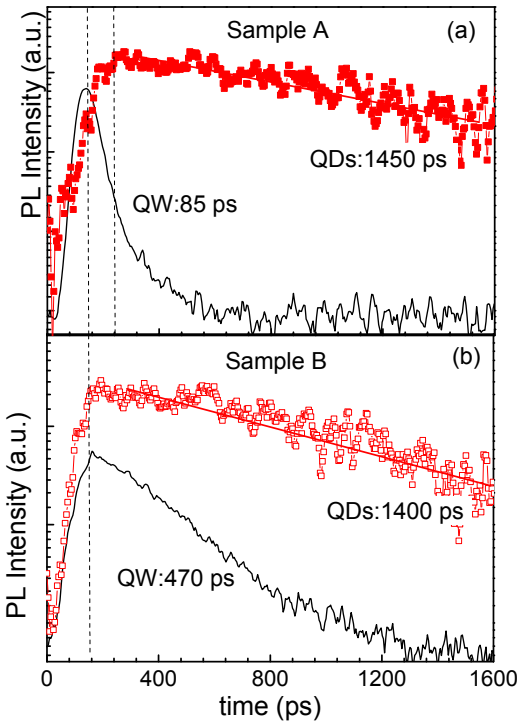
Sample A
(a)
PL Intensity (a.u.)
QDs:1450 ps
QW:85 ps
Sample B
(b)
PL Intensity (a.u.)
QDs:1400 ps
QW:470 ps
0
400
800
1200
1600
time (ps)